Case Studies in Thermal Engineering 65 (2025) 105657

Contents lists available at ScienceDirect

Case Studies in Thermal Engineering

journal homepage: www.elsevier.com/locate/csite

Heat transfer characterization of a new collector design featuring ribs, petals, and helical twisted tapes: Experimental study

Banw Omer Ahmed [a], Adnan Ibrahim [a,*], Hariam Luqman Azeez [a], Sharul Sham Dol [b,**], Ali H.A. Al-Waeli [c], Mahmoud Jaber [a]

[a] *Solar Energy Research Institute, Universiti Kebangsaan Malaysia, 43600, Bangi, Selangor, Malaysia*
[b] *Department of Mechanical and Industrial Engineering, Abu Dhabi University, Abu Dhabi, PO Box 59911, United Arab Emirates*
[c] *Engineering Department, American University of Iraq, Sulaimani, Kurdistan Region, Sulaimani, Iraq*

ARTICLE INFO

Handling Editor: Huihe Qiu

Keywords:
Surface with ribs
Petal arrangement
Helical inserter
Silicon carbide-enhanced nanofluid
Thermohydraulic Performance Factor

ABSTRACT

The limited thermal efficiency of collectors in photovoltaic thermal systems continues to pose a major hurdle. This study tackles the issue by developing an innovative collector featuring a rib and petal arrangement, combined with a helical twisted tape and channelling silicon carbide-enhanced nanofluids at volume concentrations of 0.3 %, 0.6 %, and 0.9 %. Thermohydraulic Performance analysis evaluates five absorber tubes: a smooth tube, a ribbed and petaled tube, and versions with added coil, twisted tape, and both coil and twisted tape. The study also examines the thermal efficiency of the corresponding collectors of each absorber tube. Flow rates of 0.01–0.085 kg/s, a heat flux and solar irradiances of 400 W/m^2, and varying concentrations of nanofluid are the primary conditions of the experiments. Results indicate that mass flow rate positively correlates with the Nusselt number and thermal efficiency but negatively correlates with the Friction Factor and Thermohydraulic Performance Factor. The new design of this study records a maximum Thermohydraulic Performance enhancement of 1.5 times compared to a smooth tube and an optimal thermal efficiency enhancement of 20.4 % in comparison to a smooth tube collector. In the best case, there is a decline of 50.1 % in the Thermohydraulic Performance Factor and an increase of 10.2 % in thermal efficiency when the mass flow rate increases.

1. Introduction

In the 21st century, a major objective for both industries and scientific communities is to integrate sustainability principles into their outcomes [1,2]. Sustainability focuses on maximizing production while safeguarding natural resources, protecting the environment, and considering social and economic factors [3]. Researchers are actively exploring innovative approaches to fluid flows and heat transfer in channels to enhance production efficiency while minimizing costs, pollution, and energy waste [4]. Passive cooling techniques exemplify methods that align closely with sustainability principles [5]. These techniques significantly improve thermal efficiency without the need for external energy sources or hazardous materials [6]. The use of passive cooling is widespread, but the integration of ribbed designs in absorber tubes represents a particularly promising area of research, offering substantial benefits with minimal drawbacks [7]. Additionally, research has shown that incorporating coils, twisted tapes, and nanofluids will bring about

* Corresponding author.
** Corresponding author.
E-mail addresses: iadnan@ukm.edu.my (A. Ibrahim), sharulshambin.dol@adu.ac.ae (S.S. Dol).

https://doi.org/10.1016/j.csite.2024.105657
Received 19 September 2024; Received in revised form 23 November 2024; Accepted 14 December 2024
Available online 16 December 2024

additional benefits [8–10].

Recent research has focused on enhancing the heat transfer performance of absorber tubes by incorporating ribs. These ribs are meticulously designed extensions that enhance turbulence in the flow, expand the contact surface, and optimize the flow distribution [11]. As a result, they significantly improve heat transfer efficiency and overall thermal performance [11]. Deshmukh and Lashane [12] have investigated the thermal performance of a curved rib inside an absorber tube. The experiment was performed over Reynold number range of 10000 and 50000. Their results showed that the heat transfer coefficient increased by 120 %–450 % when compared to a smooth tube. Zhu et al. [13] examined how annular ribs in absorber tubes perform and found that their innovative design improves heat transfer coefficient by 38 % with inner ring ribs. The result of their novel design showed that the heat transfer efficiency increases by 38 % with inner ring ribs. In another attempt, Wang et al. [14] used numerical and experimental approaches to analyse the heat transfer coefficient of non-uniform wavy ribs absorber tubes with a Reynold number ranging from 10000 to 40000. The absorber tube with wavy ribs exhibited a 22.6 % increase in the Nusselt number when compared to a smooth tube. Kumar and Ibraham [15] studied the effect of circular ribs on the surface of the inner tube in the application of a double-pipe heat exchanger. Their results indicated that the design achieved a maximum Nusselt number of 2.48 at a Reynolds number of 5000. Lastly, Fu et al. [16] enhanced the thermal performance of an absorber tube using W-shaped micro-ribs. The result of the heat transfer performance showed an increase of 39.7 %–48.9 % at Reynold number 4000–10000. All these studies and many others confirm the effectiveness of ribs in boosting the thermal efficiency of absorber tubes.

Aside from improving the surface condition of the absorber tube, researchers use twisted tapes or coils inside the tube to create more vortexes in the flow. The formation of vortexes has been proven to increase heat transfer augmentation significantly [17]. For instance, Mehata et al. [18] employed a twisted tape in their new design of a solar collector. They tested their new design under Reynold numbers ranging from 1000 to 9000. Their findings indicated that the incorporation of twisted tape increases Nusselt number by 316 % while the thermal performance of the new design is enhanced by 12.2 %. In another attempt to boost the electrical and thermal performance of a photovoltaic thermal collector, Goksu et al. [19] used a special twisted tape in Reynold number range of 500–1900. Their findings revealed that the system improved electrical efficiency by 15.59 % and thermal efficiency by 59.35 %. Lastly, Nilpueng et al. [20] studied the effect of incorporating twisted tapes into absorber tubes on pressure drop. They found that it decreased the pressure drop of their absorber tube design by 34.8 %, especially at low Reynold number values.

Another way to increase the thermal performance of absorber tubes via creating vortex formation is by employing a coil instead of a twisted tape. For instance, Sharaf et al. [21] numerically studied the impact of a spring wire on the thermal performance of an absorber tube. The results demonstrated a high increase in Nusselt number, calculated to be 174 %, compared to a smooth tube at Reynold number range between 4500 and 7000. To extend their previous work, Sharaf et al. [22] used multi-spring wires and recalculated for Nusselt number, Friction Factor, and exergy efficiency. Their findings showed a noticeable increase of 112 %, 134 %, and 61 %, respectively, compared to a smooth tube at the Reynold number range of 4500–7500. Lastly, Ibrahim et al. [23] experimentally evaluated the heat transfer augmentation by inserting a wire coil into a plain tube. The results indicate that the Nusselt number increased by five times and the thermal performance ratio by 2.2 compared to a smooth tube at Reynold number range between 6000 and 20000.

With all the accomplishments reported in the literature with using coils and twisted tapes in channel designs, the recent literature highlights the synergetic impact of combining coils and twisted tapes. The combined designs guarantee the creation of more turbulences and expand the contact area. Farhadi et al. [24] numerically and experimentally studied heat transfer augmentation by using a reverse coil with twisted tape. The study was conducted at laminar region (Reynold number between 10 and 2000) and turbulent region (Reynold number between 12000 and 18000). The study found that the updated design achieved a higher heat transfer ratio of 1.55 compared to using the techniques separately. Azeez et al. [25] investigated the effect of helical twisted tape in a petaled arrangement and dimpled absorber tube, which was used as a collector for a photovoltaic thermal system. The findings of the new tube indicated a significant improvement in the overall energy and exergy efficiency of the system, which reached 11.7 % and 15.3 %, respectively.

While surface enhancement techniques are highly effective and cost-efficient, researchers have sought additional ways to boost the performance of absorber tubes. One promising approach is the use of nanofluids (NF) instead of water [26]. NFs are advanced fluids containing suspended nanoparticles, typically metals or metal oxides, which significantly enhance thermal conductivity and heat transfer efficiency [27]. For instance, M. Sheikholeslami et al. [28] used a co-friendly NF in their new design of photovoltaic thermal. The primary condition of their test was fluid velocity of 0.01 and 0.18 m/s and solar irradiance of 800 W/m^2. Their findings indicated that the maximum exergy performance was 15.32 %, while the electrical and thermal performances were 14.05 % and 55.22 %, respectively. All these values were higher than those achieved with water alone. In another study, Jabeen et al. [29] used silicon carbide-based NF in their new design of a solar collector, and they reported a 45.13 % increase in the thermal efficiency of the new design. Sofiah et al. [30] used hexagonal boron nitride enhanced NF in their new design of photovoltaic thermal. The results indicated that the system achieved an electrical efficiency of 5.73 %–5.88 %, a thermal efficiency of 54.15 %–62.73 %, and an overall efficiency of 59.88 %–68.62 %. Lastly, Maseer et al. [31] used aluminum oxide-enhanced NF instead of water in a photovoltaic thermal system. They have reported that the NF was able to reduce the surface temperature by 29.93 % compared to the surface temperature of a bare PV. It also enhanced the electrical, thermal, and total efficiencies of the system by 12.70 %, 78.99 %, and 91.83 %, respectively.

Nomenclature

A	Cross-sectional area of the pipe (m^2)	ST	Smooth tube

(*continued on next page*)

(*continued*)

CP	Specific heat (J/Kg K)	$THPF$	Thermohydraulic Performance Factor
d_{bf}	Density of based fluid (Kg/m^3)	T_{in}	Inlet temperature (K)
D_h	Hydraulic diameter (m)	T_{out}	Outlet temperature (K)
d_{np}	Density of nanoparticle (Kg/m^3)	T_{wall}	Wall temperature (K)
h_i	Convective heat transfer coefficient(W/m^{2}K)	**Greek Symbols**	
K_{bf}	Thermal conductivity of based fluid (W/M. K)	u	Velocity (m/s)
K_{nf}	Thermal conductivity of nanofluid (W/M. K)	λ	Thermal conductivity (W/M. K)
K_{np}	Thermal conductivity of nanoparticle (W/M. K)	$\varnothing$	Nanoparticle volume fraction %
L	Length of the pipe (m)	ρ_{nf}	Nanofluid density (Kg/m^3)
N	Avogadro number	ρ_{bf}	Based fluid density (Kg/m^3)
Nu_i	Nusselt number	ρ_{np}	Nanoparticle density (Kg/m^3)
Q_u	Heat obtained (W)	μ	Dynamic viscosity (Pa. s)
Re	Reynolds Number	μ_{nf}	Viscosity of the nanofluid (pa. s)
RPT	Ribbed and petaled arrangement tube	μ_{bf}	Viscosity of based fluid (Pa. s)
RPTC	Ribbed and petaled arrangement tube + coil	$ʆ$	Friction factor
RPTTT	Ribbed and petaled arrangement tube + Twisted tape	ρ	Density (Kg/m^3)
RPTHTT	Ribbed and petaled arrangement tube + helical twisted tape	ΔP	Pressure drops
		$\dot{m}$	flow rate of fluid (kg/s)

Even though literature has documented a lot of studies that have attempted to increase the overall performance of a collector in a photovoltaic system, there are still gaps regarding developing a collector design that balances exceptional thermal performance and cost-effectiveness.

- This study develops a new absorber tube-based collector that features ribs and petal arrangement on its surface, integrates a helical twisted tape, and channels water and three different concentrations of NF.

The study determines the heat transfer characteristics and thermal performance of five tubes, namely smooth tub (ST), ribbed and petaled arrangement tube (RPT), ribbed and petaled arrangement tube integrated with a coil (RPTC), ribbed and petaled arrangement tube integrated with a twisted tape (RPTTT), and ribbed and petaled arrangement tube integrated with a helical twisted tape (RPTHTT) along with their corresponding collector designs. Additionally, it will use silicon carbide-enhanced NF in three concentrations of 0.3 %, 0.6 %, and 0.9 % to further boost the heat transfer characteristic and thermal efficiencies of the best-selected absorber tube and its corresponding collector design. The study was conducted under a constant heat flux of 400 W/m^2 with varying mass flow rates in the range of 0.02–0.085 kg/s. It is expected that the new absorber tube developed in this study will significantly contribute to enhancing the thermal performance of the collector's design in photovoltaic thermal systems.

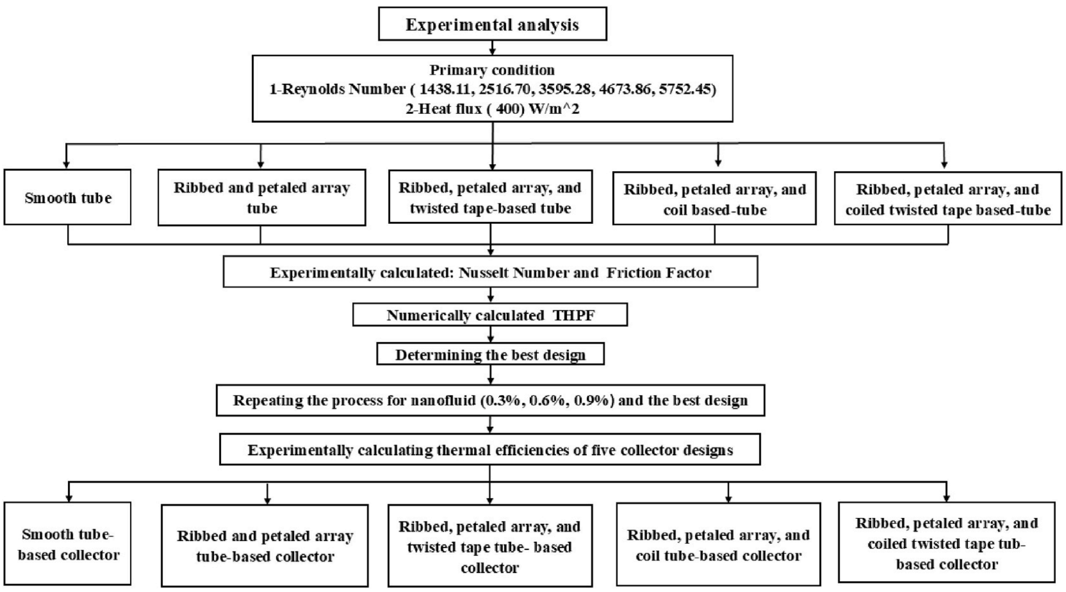

Fig. 1. The diagram of the methodology adopted in this research.

2. Methodology

As it is demonstrated in Fig. 1, the methodology adopted for this study follows four main steps. First, Nusselt number and Friction Factor are experimentally collected for five tube designs, namely an ST, RPT, RPTC, RPTTT, and RPHTT. Subsequently, the values of THPF are numerically calculated for the five cases. Once the best design is chosen, the same two first steps are repeated for NF with 0.3 %, 0.6 %, and 0.9 % volume concentration of SiC nanoparticles. Finally, the thermal efficiencies of all the absorber tube-based collectors are experimentally calculated.

2.1. The new design description

The novel absorber tube design, made from aluminium, incorporates several innovative features aimed at enhancing heat transfer augmentation. The design includes 32 rectangular ribs evenly spaced around the surface of a circular tube. These ribs are anticipated to increase turbulence and expand the surface contact area [32]. To further disrupt the flow, petal arrangement is integrated into the ribs' surfaces. Ribs and petal arrays, when put together, are expected to significantly enhance performance by increasing the contact area, disrupting thermal boundary layers, and inducing greater turbulence, thereby improving heat transfer and overall system efficiency. Additionally, a helical twisted tape is inserted into the tube to induce a vortex, which further improves heat transfer [32]. The literature indicates that the simultaneous incorporation of coils and twisted tapes yields superior performance compared to their individual application. This can be attributed to the coiled twisted tape's ability to not only increase the contact area but also enhance vortex generation and turbulence formation more effectively than either component used independently [32]. Fig. 2 A and B illustrate both the pictorial and geometrical details of the absorber tube and its collector design.

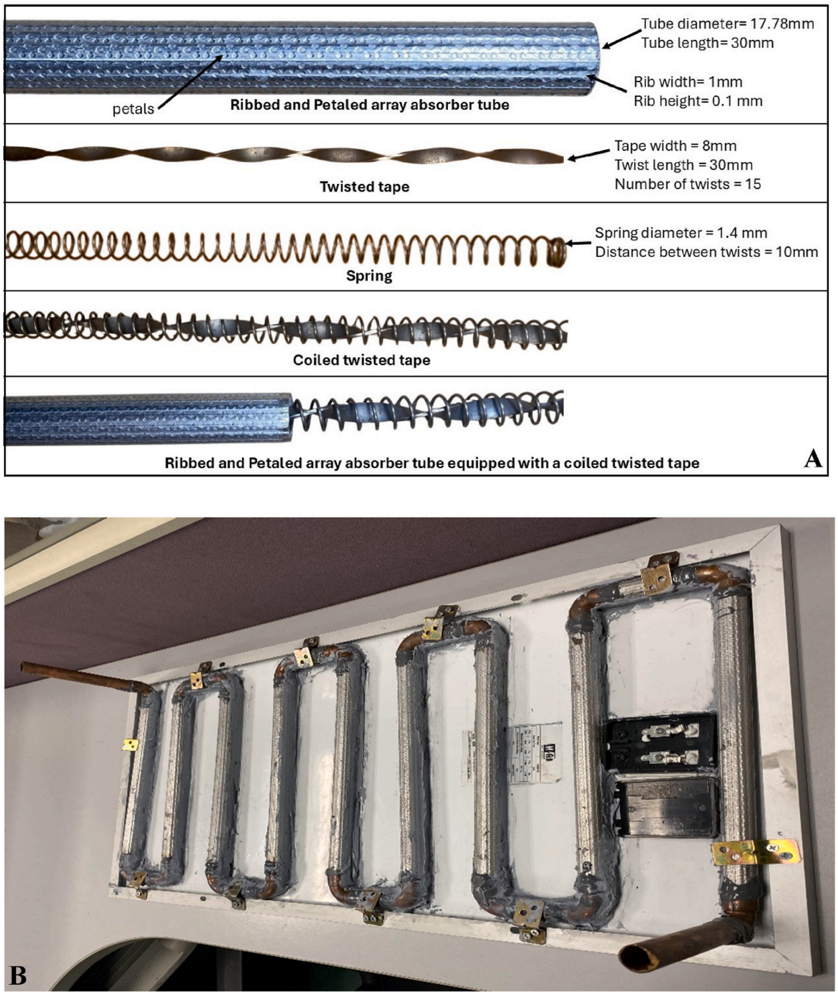

Fig. 2. Details and pictorial demonstration of (A) a new absorber tube and (B) its corresponding collector.

2.2. Nanofluid preparation process

Before starting the experiment, the study prepared NF with 0.3 %, 0.6 %, and 0.9 % volume concentrations of SiC. To create the concentrations, 694.8 g of SiC powder were mixed into 24 L of water for the 0.9 % solution, 463.2 g were used for the 0.6 % solution, and 231.6 g for the 0.3 % solution. These quantities were determined using Equation (1), with all variables defined in the nomenclature [33]. Additionally, polyvinylpyrrolidone was added as a surfactant to improve the dispersion of the SiC particles. Detailed information about the SiC nanopowder used in the experiment can be found in Table 1. After placing all the components in the container at the correct proportions, they were mechanically mixed for 10 min. After that, the mixture underwent ultrasonic treatment in a bath for 3 h at 85 °C, with a vibration frequency of 60 Hz, to achieve complete uniformity [25]. Fig. 3 depicts the NF prepared for this study.

$$\phi = \frac{\frac{m_p}{\rho_p}}{\frac{m_p}{\rho_p} + \frac{m_f}{\rho_f}} \tag{1}$$

2.3. The characterization and thermophysical properties of the nanofluid

Once the preparation process was completed, the samples underwent testing and analysis of their thermophysical properties to confirm their preparation quality and effectiveness. Field Emission Scanning Electron Microscopy (FESEM) was used for imaging, mapping, and analysis. As shown in Fig. 4, the nanoparticles are evenly distributed in the base fluid, comprising 50.3 % Si, 42.2 % C, and 6.3 % O_2. The particles are cubic and measure between 56 and 58 nm. These observations align with previous studies [34,35]. The thermophysical properties of the NF, including density, viscosity, and thermal conductivity, were measured across a temperature range of 15–50 °C using the Anton Paar model DMA 1001 for density, the Anton Paar model MCR 92 viscometer, and Linsey's model THB-500. All the obtained results are documented in Table 2. Equations (2)–(5) were used to validate the results numerically. Equation (6) was applied to determine the specific heat capacity of the sample. The thermophysical results obtained in this study are similar in values to previous studies in the literature [36]. The nomenclature includes definitions for all parameters used in Equations (2)–(6) [37].

$$\rho_{nf} = (1 - \phi)\rho_{bf} + \phi\rho_{np} \tag{2}$$

$$\mu_{nf} = \mu_{bf} \times \frac{1}{\left(1 - 3.87\left(\frac{d_{np}}{d_{bf}}\right)^{-0.3} \times \phi^{1.03}\right.} \tag{3}$$

$$d_{nf} = \frac{6M}{N \times \pi \times \rho_{nb}} \tag{4}$$

$$K_{nf} = \frac{K_{np} + 2K_{bf} + 2\phi(K_{np} - K_{bf})}{K_{np} + 2K_{bf} - 2\phi(K_{np} - K_{bf})} \times K_{bf} \tag{5}$$

$$CP_{mix} = \frac{(1 - \phi)(\rho CP)_{water} + (\phi\rho CP)_{np}}{\rho_{mix}} \tag{6}$$

The FESEM and the thermophysical properties of NF, on one hand, and the fact that there was no sedimentation observed in the NF solution after one month, all confirmed that the prepared NF had a good distribution of nanoparticles in the based fluid. Moreover, it is a good guarantee of stability and high performance, too.

Table 1
The thermophysical details of the nanoparticle that has been used in this study.

Thermophysical properties of SiC	
Name of the manufacturer	US Res. Nanomaterials
Appearing color of the nanoparticle	Greyish white
Level of purity of the sample	99+%
PH value	3-7 at 20 °C
Shape of the nanoparticle	Cubic
Determine the melting point of the sample	2744 °C
size of one particle	39–61 nm
Thermal Conductivity	369–489 W/m. K
Bulk Density	3.21 g/cm^3
Zeta potential	27.8 mV

Fig. 3. Preparation process of the SiC enhanced NF.

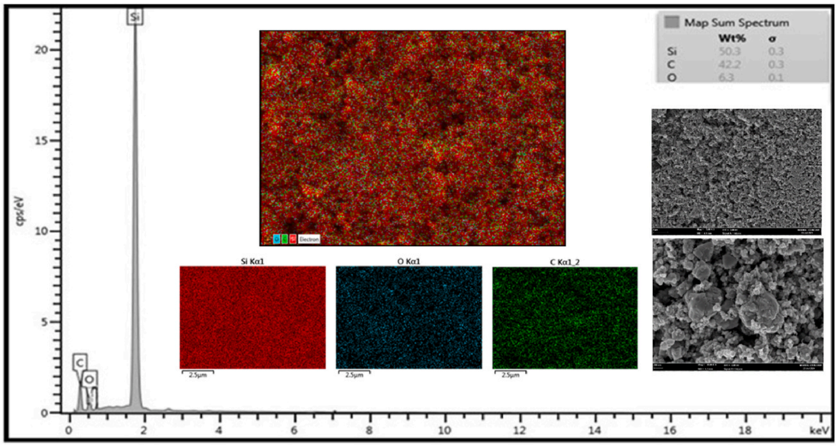

Fig. 4. The FESEM images, maps, and analysis of the nano solutions prepared in the study.

Table 2
The calculated density, viscosity, and thermal conductivity of the prepared NFs of the study.

Temp (°C)	Water			0.3%SiC-enhanced NF			0.6%SiC-enhanced NF			0.9 % SiC-enhanced NF		
	ρ (kg/m^3)	μ (Pa. s)	K (W/M. K)	(ρ kg/m^3)	(μ Pa. s)	(K W/M. K)	(ρ kg/m^3)	(μ Pa. s)	(K W/M. K)	(ρ kg/m^3)	(μ Pa. s)	(K W/M. K)
15	999.2	1.12	0.56	1006.7	1.39	0.62	1013.5	1.48	0.64	1025.5	1.52	0.67
20	998.3	1.13	0.58	1006.2	1.36	0.63	1012.9	1.47	0.66	1023.6	1.51	0.69
25	997.1	1.08	0.60	1005.1	1.29	0.65	1011.9	1.39	0.68	1021.6	1.48	0.72
30	995.8	0.99	0.62	1003.1	1.19	0.67	1010.5	1.27	0.69	1020.5	1.36	0.74
35	994.2	0.89	0.64	1001.4	1.11	0.69	1008.9	1.18	0.71	1019.8	1.24	0.76
40	992.3	0.80	0.66	999.2	1.01	0.7	1006.8	1.08	0.73	1018.6	1.13	0.78
45	990.2	0.74	0.67	997.	0.97	0.71	1003.6	0.99	0.74	1017.8	1.01	0.80
50	987.8	0.73	0.68	994.1	0.98	0.72	1000.6	1.01	0.75	1016.8	0.99	0.81

2.4. The experimental rig

Once the samples were prepared, they were set up for the experiment. First, five thermocouples were attached to the sample to record the temperature at five different points on the pipe wall. Next, the sample was wrapped with a silicon rubber heater with a power density of 400 W/m^2, and a voltage regulator monitored the heat flux. An insulating layer was then added around the sample to trap heat and facilitate handling. With the sample prepared, the five thermocouples were connected to an AT47V data logger. Additionally, two RTD sensors were placed at the inlet and outlet of the sample and connected to the data logger. This setup allowed the data logger to monitor the inlet and outlet fluid temperatures as well as the wall temperature of the tube. A DPG 409 digital differential pressure gauge was installed at both the inlet and outlet of the sample to measure pressure accurately. The fluid circulation was controlled and cooled using a cooler, mass flow meter, heat exchanger, and two fluid pumps. Fig. 5 (A and B) provides a schematic and pictorial representation of the system. The experimental setup illustrated in Fig. 5 (C) was employed to determine the thermal efficiency of the collectors. The experiment was conducted under identical solar irradiance of 400 W/m^2, and RTD sensors were used to measure the inlet and outlet temperatures of the collectors. It is noteworthy that this setup is specifically designed to collect data

Fig. 5. (A) the schematic diagram, (B) the pictorial demonstration of the experimental setup for the tubes, and (C) the setup for the collector.

related to both the electrical and thermal performance of photovoltaic thermal (PVT) systems. However, for the purposes of the present study, data collection was limited to the temperature differentials of the collectors. These measurements were sufficient to calculate the thermal efficiency of the examined collectors, aligning with the study's focus on thermal performance analysis alone.

2.5. *The models of the study*

The study used Thermohydraulic Performance Factor (THPF) analysis-based models to perform all its calculations under varying mass flow rates of 0.01–0.085 kg/s and constant heat flux of 400 W/m^2. The recorded mass flow rates of the study were converted into velocity values using Equation (7) [37].

$$u = \frac{\dot{m}}{\rho A} \tag{7}$$

Dynamic viscosity and velocity of the fluid helped in determining the Reynold number of the fluid through Equation (8) [37]. The value of Reynold's number will be crucial for the coming steps and overall description of the newly designed absorber tubes.

$$Re = \frac{\rho D_h u}{\mu} \tag{8}$$

The RTD sensors determined the exact inlet and outlet temperature of the fluid, which, with the help of Equation (9) [38], determined the heat gain of the system.

$$Q_u = \dot{m}\, CP\, (T_{out} - T_{in}) \tag{9}$$

The thermocouples determined the wall temperature of the samples, and Equation (10) calculated the convective heat transfer coefficient of the samples [38].

$$h = \frac{Q_u}{\left(T_{wall} - \left(\frac{T_{out} - T_{in}}{2}\right)\right)A} \tag{10}$$

Once the convective heat transfer coefficient is known, Equation (11) can calculate the Nusselt number of the samples, which is a very important outcome in describing the heat transfer characteristic of any system [38].

$$Nu_i = \frac{h_i D_h}{\lambda} \tag{11}$$

Nusselt number on its own cannot give a full description of the heat transfer characteristics of any system unless the Friction Factor is provided. The Friction Factor and Nusselt number are opposite to one another, and their effects must be considered simultaneously. Equation (12) will calculate the Friction Factor with the help of the pressure gauge inserted in the system [38].

$$\int = \frac{2\Delta P}{\rho u_i^2}\frac{D_h}{L} \tag{12}$$

The THPF must be performed to optimize between the Friction Factor and Nusselt number, which are opposite to one another. Equation (13) calculates the THPF of the samples [38].

$$THPF = \frac{(Nu_i / Nu_{i)}}{(\int / \int)^{\frac{1}{3}}} \tag{13}$$

Lastly, Equation (14) was used to calculate the thermal efficiencies of all the collector designs studied in this research.

Table 3
The instruments used in the experiment with their uncertainty percentages.

$$W_R = \left[(0.2)^2 + (0.15)^2 + (0.15)^2 + (0.5)^2 + (0.08)^2 + (0.2)^2\right]^{0.5}$$

$$W_R = 0.617\%$$

Instrument	Model	uncertainty
Datalogger	AT47V	0.2 %
RTD sensor	PT 100	0.15 %
Thermocouple (wire sensor)	K-type	0.15 %
Digital flow meter	DHYB-800	0.5 %
Digital Differential Pressure Gauge	DPG409	0.08 %
Cooling Unit	SPH20	0.2 %

$$\eta_{th} = \frac{Q_u}{I \times A_{collector}} = \frac{\dot{m} \times C_p(T_{out} - T_{in})}{I \times A_{collector}} \tag{14}$$

2.6. Uncertainty analysis

Lastly, the percentage of uncertainty of the experiment must be revealed so that the result of the experiment can be duplicated with a certain range of mistakes. Below is the percentage of uncertainty of the experiment calculated through Equation (15) and Table 3 [39].

$$W_R = \left[\left(\frac{\partial R}{\partial X_1} W_1 \right)^2 + \left(\frac{\partial R}{\partial X_2} W_2 \right)^2 + \ldots \left(\frac{\partial R}{\partial X_n} W_n \right)^2 \right]^{0.5} \tag{15}$$

3. Results and discussion

As discussed previously, this study will investigate the heat transfer characterization of five different absorber tube designs using water and NF at Reynold number range of 1400–5800 and a constant heat flux of 400 W/m^2. The experimentally calculated parameters will be Nusselt number, Friction Factor, THPF, and thermal efficiency.

3.1. The analysis of Nusselt number

As it was mentioned previously, the study will meticulously record the Nusselt number values for all the five designs included in this study. The result has shown that there is a positive relationship between Nusselt number and mass flow rate, which is consistent with the literature [40]. The findings also show that compared to ST, the other tubes, such as RPT, RPTC, RPTTT, and RPTHTT, increase Nusselt number value by 19.1 %, 28.6 %, 32.2 %, and 46.7 %, respectively. As it was explained previously, the reason for such improvement can be contributed to many factors, such as surface condition improvement, creating more turbulence in the flow, inducing the formation of vortexes, etc [41]. Fig. 6 shows the values of the Nusselt number for all the cases of this study.

3.2. The analysis of the Friction Factor

The study also determined the Friction Factor for all cases examined. Consistent with existing literature, which indicates a negative relationship between the Reynolds number and the Friction Factor, the findings of this study are consistent with the reported results of the literature [42]. Nevertheless, the ST design recorded the least Friction Factor value while the order for the other are RPT, RPTC, RPTTT, and RPTHTT. From the results provided in Fig. 7, it can be concluded that as the design gets more complicated in terms of surface improvement and inserts, the Friction Factor increases too, and this aligns with reports of studies available in the literature [43]. The percentage of increase in Friction Factor compared to ST is 3.78 % for RPT, 6.68 % for RPTC, 12.2 % for RPTTT, and 34.9 % for RPTHTT.

As was shown, the values of both Nusselt number and Friction Factor increase as the designs are modified with better passive cooling techniques. However, the best design is the one that maximizes Nusselt number and minimizes the Friction Factor. Therefore, an optimization study must be conducted to reveal which design has the best performance. Equation (12) shows how THPF analysis can perform the optimization and determine the best design in terms of heat transfer augmentation.

3.3. The Thermohydraulic Performance Factor analysis

The THPF analysis seeks to optimize the effect of two opposing parameters, which are Nusselt number and Friction Factor. As shown in Fig. 8, the study lists the tubes as follows in terms of having the best thermal performance, namely the RPT, RPTC, RPTTT, and RPTHTT. Compared to RPT, the THPF for the RPTC is higher by 10.8 %, while it is higher by 14.9 % and 24.9 % for the RPTT and the RPTHTT. It should also be mentioned that all the designs of this study record higher THPF values at low Reynold numbers. For

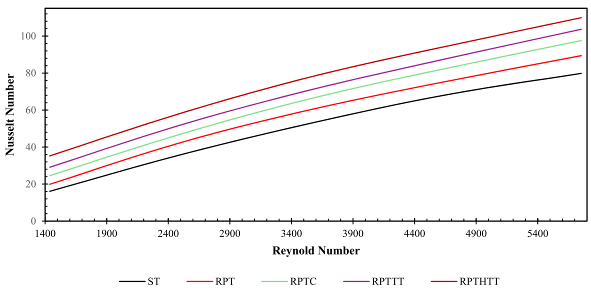

Fig. 6. The correlation between Nusselt number and Reynold number using water as coolant.

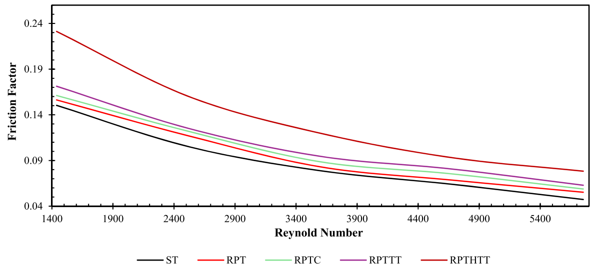

Fig. 7. The correlation between Friction Factor and Reynold number using water as coolant.

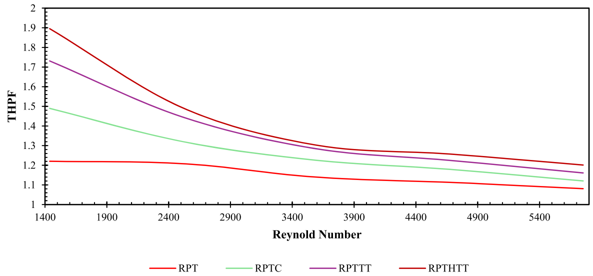

Fig. 8. The correlation between THPF and Reynold number using water as coolant.

instance, as Reynold number increases from 1400 to 5800, the designs face declines in THPF by 7.8 % for the RPT, 17.5 % for RPTC, 21.1 % for RPTTT, and 26.6 % for RPTHTT.

3.4. The effect of nanofluid with various concentrations

To further increase the effectiveness of the best absorber tube determined in the previous section, the study will replace water with SiC-enhanced NF in volume concentrations of 0.3 %, 0.6 %, and 0.9 %. The same experimental and numerical steps were repeated to collect data for the NF case. As it is shown, Fig. 9 A presents Nusselt number values for the three NF cases. Compared to the best case with water and the RPTHTT, the 0.3 %, 0.6 %, and 0.9 % concentration of SiC increased Nusselt number by 26.13 %, 39.8 %, and 44.3 %, respectively. The reason for the recorded improvement is the improvement in the thermophysical properties of the NF samples which have been shown in Table 2.

Even though there is a positive relationship between the concentration of nanoparticles and the values of the Nusselt number, the experimental results shown in Fig. 9 B indicate that higher nanoparticle concentrations cause the Friction Factor to increase. The percentage of Friction Factor increase of 0.3 %, 0.6 %, and 0.9 % compared to using water and the RPTHTT are 11.2 %, 26.7 %, and 36.45 %, respectively. The reason is attributed to the fact that higher nanoparticle concentration leads to more friction being produced between the wall surface of the tubes and the nanoparticles. With the data provided in Fig. 9A and B, THPF optimization must be conducted again to reveal which nanoparticle concentration works the best with the newly designed absorber tube developed in this study.

Fig. 9C shows the results of the THPF analysis of the three included concentrations of nanoparticles in the study. The data reveals that the NF with 0.9 % concentration of SiC increases the THPF the most while the 0.6 % and 0.3 % are the second and the third most effective. Compared to employing water and the RPTHTT, THPF enhancement is 23.2 %, 33.3 %, and 35.3 % for the 0.3 %, 0.6 %, and 0.9 % nanoparticle concentrations, respectively. Additionally, it was again confirmed that the three concentrations of nanoparticles perform the best at low Reynold number values. As Reynold number increases from 1400 to 5400, the value of THPF declines by 43.1 %, 49.7 %, and 50.1 % for 0.3 %, 0.6 %, and 0.9 % concentrations of nanoparticles, respectively.

3.5. The thermal efficiencies analysis of the collector designs

The study calculated the thermal efficiencies of five collector designs, namely ST-based collector, RPT-based collector, RPTC-based collector, RPTTT-based collector, and RPTHTT-based collector. Compared to an ST-based collector, thermal efficiencies enhancement of 5 %, 6.5 %, 7.2 %, and 6.1 % were recorded for RPT-based collectors with water, and SiC-enhanced NF with 0.3 %, 0.6 %, and 0.9 % volume concentration, respectively. In the cases of employing a coil, the enhancement went up to 10.7 %, 11.7 %, 12.03 %, and 11.7 %, while inserting the twisted tape alone recorded enhancement of 15.7 %, 15.9 %, 16.4 %, and 15.5 % for water, 0.3 % SiC, 0.6 % SiC, 0.9 % SiC enhanced NF. Finally, inserting the coil and the twisted tape simultaneously with the new tube designed recorded thermal efficiency enhancement of 20.2 %, 20.3 %, 19.8 %, and 18.9 %, respectively. Fig. 10 shows all the calculated thermal efficiencies of the cases studied in this research. Therefore, it is once again confirmed that the selected design of this study records the best thermal

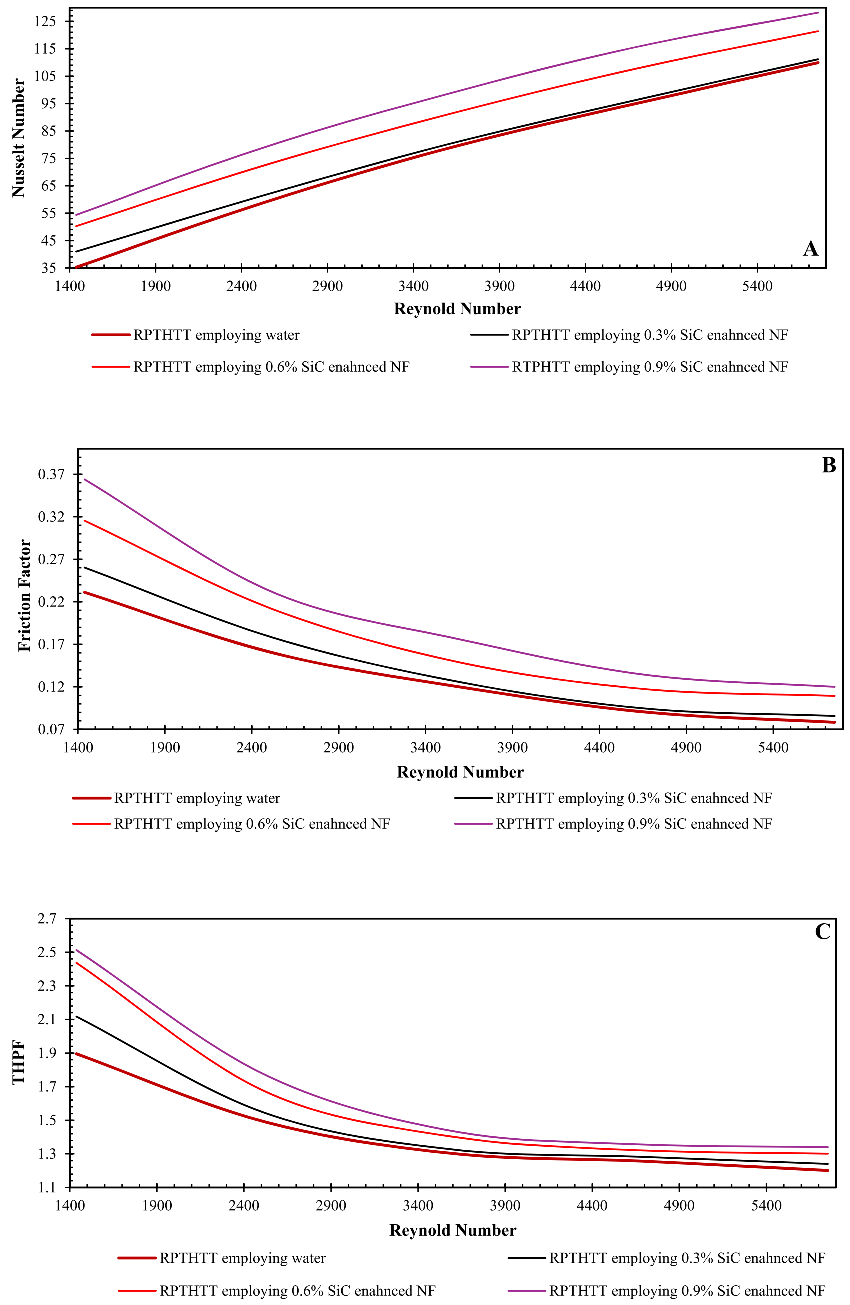

Fig. 9. The correction between A) Nusselt number, B) Friction Factor, and C) THPF and Reynold number for NF cases.

efficiencies over all the coolant types included in the study.

Even though the calculation of the tubes alone showed that the performance of all the tubes is better at a low Reynolds number, which was calculated to be about 50.1 %, the relationship becomes reversed for the collector. As the mass flow rate goes up, there is an optimal enhancement of 10.2 %. The reason here is that the size of the collector is significantly bigger which enables more heat absorption by the fluid and results in a higher outlet temperature of the fluid. Finally, Table 4 compares the thermal efficiency obtained for the newly designed collector with some other designs of the current literature.

4. Conclusion

As demonstrated previously, the main objective of this study was to reveal the heat transfer characteristics of five absorber tubes and their corresponding collector designs under the primary condition of applying varying Reynold numbers of 1400–5400, constant

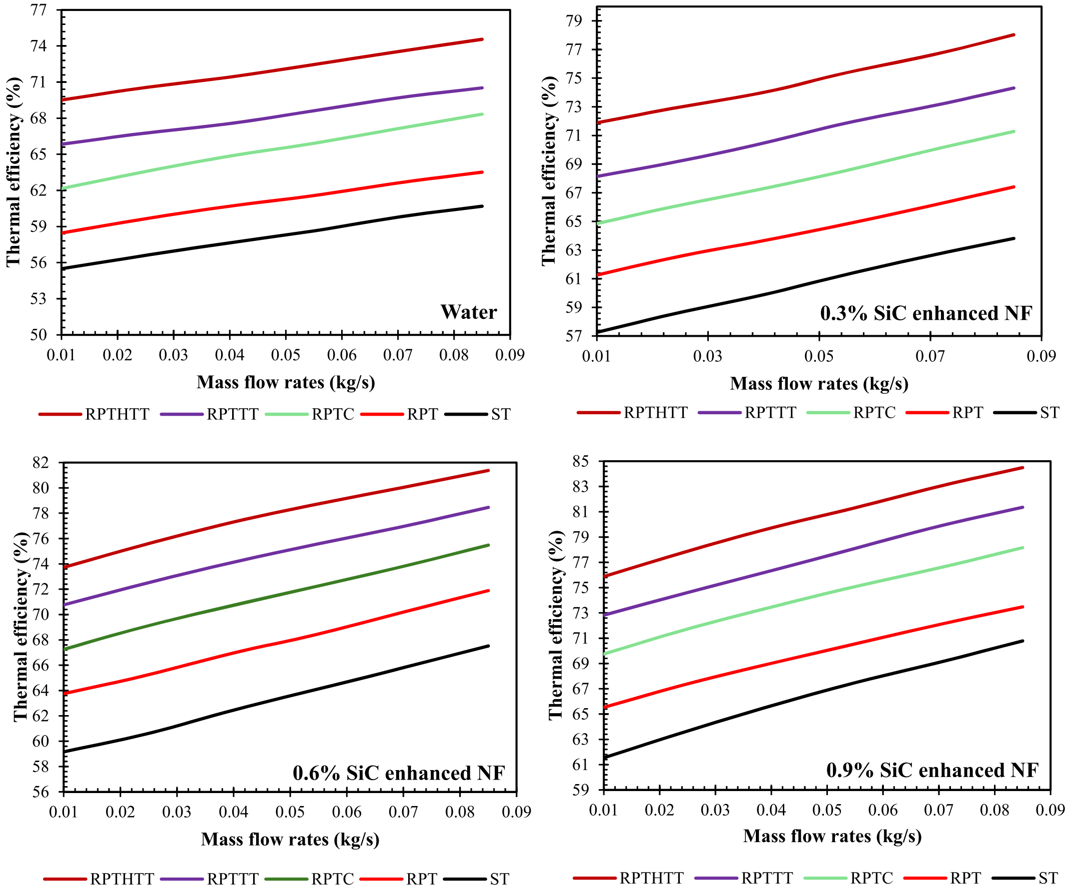

Fig. 10. The thermal efficiencies calculated for all the cases of the study.

Table 4
Comparing the thermal efficiency of the current study with newly published articles on the same topic.

Ref and year	Types of study	Coolant types & Flow rates	Thermal efficiency
[44] 2023	Experimental	Carbon oxide-enhanced NF & (60, 80 120 kg/h)	35.5 %
[45] 2023	Numerical	Water, air, finned tube & (0.01 and 0.02 kg/s)	54.25 %
[46] 2023	Experimental	Micro-fin tube and SiC-enhanced NF and PCM & (0.008–0.058 kg/s)	77.5 %
[47] 2023	Experimental	Twisted tube and SiC-enhanced NF and PCM & (0.008–0.04 kg/s)	88.2 %
[48] 2024	Experimental	Water and bi-symmetrical web flow & (0.5–2 LPM)	41 %
[49] 2024	Experimental	MWCNT/ZnO nanofluid & 0.156 kg/min	52 %
[30] 2024	Numerical	Hexagonal boron nitride-enhanced NF & (2 LPM)	54.15 %
[31] 2024	Experimental	Aluminium oxide-enhanced NF and PCM & (1–5 LPM)	78.99
The present study	Experimental	Ribs, petals, helical twisted tape, and SiC-enhanced NF (1438.11–5752.45)	84.5 %

heat flux of 400 W/m^2, and employing water, 0.3 %, 0.6 %, and 0.9 % volume concentrations of SiC enhanced NF. Employing Thermohydraulic Performance Factor analysis and thermal efficiency equation, the following results were obtained.

- There is a positive relationship between the Reynold number, with Nusselt number, and thermal efficiency, while the relationship is revered for Friction Factor and THPF.
- All the tube cases included in this study record higher THPF at low Reynold number values, while the collectors recorded the lowest thermal efficiency for the same Reynold number.
- The study lists the designs as follows in terms of THPF: ST, RPT, RPTC, RPTTT, and RPTHTT from the least to the most efficient. The same ranking persists for the thermal efficiency analysis of the collectors.
- The volume concentrations of 0.3, 0.6, and 0.9 further increased the THPF and thermal efficiencies of the designs.
- Compared to the RPT alone, the THPF is 10.8 % higher for the RPTC, 14.9 % higher with RPTTT, and 24.9 % higher with the RPTHTT.

- Compared to using water with the RPTHTT, the THPF increases by 23.2 %, 33.3 %, and 35.3 % for nanoparticle concentrations of 0.3 %, 0.6 %, and 0.9 %, respectively.
- The thermal efficiencies enhancement is 7.2 % for RPT-based collector, 12.03 % for RPTC-based collector, 16.4 % for RPTTT-based collector, and 20.3 % for RPTHTT-based collector in the best-case scenario when compared to a smooth tube.

Lastly, it is suggested that future studies investigate the following gaps that this research has not covered.

- It is suggested that the design is investigated at high Reynold number values to reveal its heat transfer characteristics.
- It is recommended that the new design is tested as a collector for a PVT system since the design is especially made for this application.
- It is advised to test the new design under high heat flux values to see its performance under higher heat flux values.

CRediT authorship contribution statement

Banw Omer Ahmed: Writing – original draft, Methodology, Formal analysis, Conceptualization. **Adnan Ibrahim:** Supervision, Methodology, Funding acquisition, Conceptualization. **Hariam Luqman Azeez:** Writing – original draft, Methodology, Formal analysis, Conceptualization. **Sharul Sham Dol:** Supervision, Methodology, Funding acquisition, Conceptualization. **Ali H.A. Al-Waeli:** Writing – review & editing, Validation, Methodology, Formal analysis. **Mahmoud Jaber:** Writing – review & editing, Validation, Methodology, Formal analysis.

Declaration of competing interest

The authors declare that they have no known competing financial interests or personal relationships that could have appeared to influence the work reported in this paper.

Data availability

Data will be made available on request.

References

[1] S.I.U. Din, A. Ibrahim, R.K. Ajeel, A. Fazlizan, A.A. Ishak, A.B. Al-Aasam, Thermal performance analysis of a double-pass solar air heater with lava rock as porous and sensible heat storage material, J. Energy Storage 95 (2024) 112564.

[2] N.J. Yusaidi, M.F. Fauzan, A.F. Abdullah, A. Ibrahim, A.A. Ishak, Theoretical and experimental investigations on the effect of double pass solar air heater with staggered-diamond shaped fins arrangement, Case Stud. Therm. Eng. 60 (2024) 104619.

[3] W.E. Ewe, K. Sopian, M. Mohanraj, A. Fudholi, N. Asim, A. Ibrahim, Exergetic performance of jet impingement bifacial photovoltaic-thermal solar air collector with different packing factors and jet distributions, Heat Tran. Eng. 45 (10) (2024) 904–914.

[4] I.O. Harmailil, S.M. Sultan, C.P. Tso, A. Fudholi, M. Mohammad, A. Ibrahim, A review on recent photovoltaic module cooling techniques: types and assessment methods, Results in Engineering (2024) 102225.

[5] A.A. Abdalkarem, A. Fazlizan, W.K. Muzammil, C.H. Lim, A. Ibrahim, K.H. Wong, H.A. Kazem, The effect of various wedge flap configurations on the performance of wind turbine airfoil, Iranian Journal of Science and Technology, Transactions of Mechanical Engineering (2024) 1–21.

[6] H. Jarimi, T. Zheng, Y. Zhang, T.R. Razak, E.Z. Ahmad, W.N.A.W. Roshdan, S. Riffat, Solar photovoltaic-assisted DC vapour compression with a low-cost ice gel thermal battery for off-grid building cooling, J. Build. Eng. 91 (2024) 109350.

[7] W.N.A.W. Roshdan, H. Jarimi, A. Ibrahim, Energetic and exergetic performance analysis of a double pass asymmetric CPC photovoltaic/thermal solar collector suitable for building facade, Int. J. Exergy 44 (3–4) (2024) 311–322.

[8] N.A.A. Affandi, N.A. Ludin, M.M. Junedi, L.C. Haw, K. Purvis-Roberts, Analysing temporal factor in dynamic life cycle assessment of solar photovoltaic system, Sol. Energy 270 (2024) 112380.

[9] T.R. Razak, H. Jarimi, E.Z. Ahmad, Simplified artificial neural network configuration in R programming for predictive modelling, in: 2023 IEEE 8th International Conference on Recent Advances and Innovations in Engineering (ICRAIE), IEEE, 2023, December, pp. 1–6.

[10] E.Z. Ahmad, T.R. Razak, H. Jarimi, Expertise-based systematic guidelines for chiller retrofitting in healthcare facilities, J. Build. Eng. 74 (2023) 106708.

[11] R.K. Ajeel, S.N. Fayyadh, K. Sopian, S.M. Sultan, W.S.I.W. Salim, C.P. Tso, Multiple impingement jets with binary hybrid nanofluids: performance assessment of flow and heat transfer characteristics, J. Therm. Anal. Calorim. (2024) 1–18.

[12] P.W. Deshmukh, S. Lahane, Numerical evaluation of novel curved rib turbulators for thermal performance improvement in circular geometries, Heat Tran. Eng. 45 (6) (2024) 528–551.

[13] C. Zhu, Z. Lin, W. Liu, Q. Liu, S. Yan, Effect of annular ribs in heat exchanger tubes on the performance of phase-change regenerative heat exchangers, Energy Sci. Eng. 11 (8) (2023) 2809–2817.

[14] L. Wang, C. Lv, J. Mao, Y. Li, D. Zhang, X. Liu, Effects of non-uniform wavy ribs on flow and heat transfer characteristics of turbine blade cooling channel, Appl. Therm. Eng. 248 (2024) 123249.

[15] Kumar, M. S., & Abraham, S. (2025). Experimental and numerical studies of detailed heat transfer and flow characteristics in the rib turbulated annulus of a double pipe heat exchanger. Int. J. Therm. Sci., 207, 109382.

[16] H. Fu, H. Sun, J. Luan, L. Yang, Y. Luan, F. Magagnato, The heat transfer enhancement mechanism of W-shaped micro-ribs on impingement cooling, Appl. Therm. Eng. (2024) 123658.

[17] J. Luo, A. Alghamdi, F. Aldawi, H. Moria, A. Mouldi, H. Loukil, S.P. Ghoushchi, Thermal-frictional behavior of new special shape twisted tape and helical coiled wire turbulators in engine heat exchangers system, Case Stud. Therm. Eng. 53 (2024) 103877.

[18] B. Mehta, D. Subhedar, H. Panchal, Z. Said, K. Sharma, M.I.H. Siddiqui, M.A. Rosen, Twisted tape inserts in parabolic trough solar collectors: assessment of Energy, Exergy, and Environmental impacts, Appl. Therm. Eng. 250 (2024) 123566.

[19] T.T. Göksu, Energy, exergy analysis, and RSM modeling of different designed twisted Tapes in placed PV/T systems, Energy 132041 (2024).

[20] K. Nilpueng, P. Kaseethong, S. Wongwises, Heat transfer and flow characteristics of a plate-fin heat sink equipped with copper foam and twisted tapes, Heliyon 10 (2024) e32307.

[21] M.A. Sharaf, S.A. Marzouk, A. Aljabr, F.A. Almehmadi, A. Kaood, S. Alqaed, Heat transfer enhancement in a double-pipe helical heat exchanger using spring wire insert and nanofluid, J. Therm. Anal. Calorim. (2024) 1–17.
[22] M.A. Sharaf, S.A. Marzouk, A. Aljabr, F.A. Almehmadi, T. Alam, D.A. Teklemariyem, Effects of multi-spring wires on hydrothermal performance of double tube heat exchanger, Case Stud. Therm. Eng. 60 (2024) 104689.
[23] F.A. Ibrahim, M.R. Muhamad, M.N. Mohd Zubir, M.B. Omar, Z. Siri, R.M. Hasan, M.M.A.A. Eid, Experimental analysis of the improvement of heat transfer in tube heat exchangers via passive flow generators using wire coil inserts, ASME Journal of Heat and Mass Transfer 146 (6) (2024).
[24] S. Farhadi, Y. Shekari, P. Omidvar, Numerical and experimental investigation of laminar and turbulent convective heat transfer in a coiled flow reverser with twisted tape insert, Int. J. Therm. Sci. 197 (2024) 108781.
[25] H.L. Azeez, A. Ibrahim, B.O. Ahmed, A.H. Al-Waeli, M. Jaber, M.A.A. Rahmat, Energy and exergy analysis of a novel collector design in a photovoltaic thermal system: an experimental study, Appl. Therm. Eng. (2024) 124125.
[26] M.A. Rahman, S.M. Hasnain, S. Pandey, A. Tapalova, N. Akylbekov, R. Zairov, Review on nanofluids: preparation, properties, stability, and thermal performance augmentation in heat transfer applications, ACS Omega 9 (30) (2024) 32328–32349.
[27] H. Babar, H. Wu, W. Zhang, T.R. Shah, D. McCluskey, C. Zhou, The promise of nanofluids: a bibliometric journey through advanced heat transfer fluids in heat exchanger tubes, Adv. Colloid Interface Sci. (2024) 103112.
[28] M. Sheikholeslami, Z. Khalili, Solar photovoltaic-thermal system with novel design of tube containing eco-friendly nanofluid, Renew. Energy 222 (2024) 119862.
[29] N. Jabeen, H.A. Haider, A. Waqas, M. Ali, An effective parametric sensitivity analysis to improve electrical and thermal energy/exergy efficiency of PVT system using nanofluid, Process Saf. Environ. Protect. 189 (2024) 1037–1051.
[30] A.G.N. Sofiah, R.K. Rajamony, M. Samykano, A.K. Pandey, J. Pasupuleti, N.F. Sulaiman, Assessment on thermophysical properties of nano enhanced heat transfer fluid with hexagonal boron nitride nanoparticles for thermal management of photovoltaic thermal (PVT) system, Process Saf. Environ. Protect. 189 (2024) 1087–1102.
[31] M.M. Maseer, F.B. Ismail, H.A. Kazem, D.M. Hachim, K.A.H. Al-Gburi, M.T. Chaichan, Performance enhancement of photovoltaic/thermal collector semicircle absorber tubes using nanofluid and NPCM, Renew. Energy 121152 (2024).
[32] B.O. Ahmed, A. Ibrahim, H.L. Azeez, S.S. Dol, A.H. Al-Waeli, M. Jaber, Energy and exergy analysis of a newly designed photovoltaic thermal system featuring ribs, petal array, and coiled twisted tapes: experimental analysis, Case Stud. Therm. Eng. (2024) 105388.
[33] R.K. Ajeel, W.I. Salim, K. Sopian, M.Z. Yusoff, K. Hasnan, A. Ibrahim, A.H. Al-Waeli, Turbulent convective heat transfer of silica oxide nanofluid through corrugated channels: an experimental and numerical study, Int. J. Heat Mass Tran. 145 (2019) 118806.
[34] A.M. Ajeena, I. Farkas, P. Víg, Energy and exergy assessment of a flat plate solar thermal collector by examine silicon carbide nanofluid: an experimental study for sustainable energy, Appl. Therm. Eng. 236 (2024), 121844. 38.
[35] A.M. Ajeena, I. Farkas, P. Víg, A comparative experimental study on thermal conductivity of distilled water-based mono nanofluids with zirconium oxide and silicon carbide for thermal industrial applications: proposing a new correlation, International Journal of Thermofluids 20 (2023) 100424.
[36] A.H. Al-Waeli, M.T. Chaichan, H.A. Kazem, K. Sopian, Comparative study to use nano-(Al2O3, CuO, and SiC) with water to enhance photovoltaic thermal PV/T collectors, Energy Convers. Manag. 148 (2017) 963–973.
[37] A. Hedau, S.K. Singal, Development of Nusselt number and friction factor correlations for double-pass solar air heater duct, Appl. Therm. Eng. 234 (2023) 121227.
[38] S. Şevik, Ö. Özdilli, M. Abuşka, Experimental investigation of relative roughness height effect in solar air collector with convex dimples, Renew. Energy 194 (2022) 100–116.
[39] A. Painuly, N.K. Mishra, P. Zainith, Heat transfer enhancement in a helically corrugated tube by employing w/eg based non-Newtonian hybrid nanofluid under turbulent conditions, J. Enhanc. Heat Transf. 29 (1) (2022).
[40] P. Saini, A. Dhar, S. Powar, Performance enhancement of fin and tube heat exchanger employing curved trapezoidal winglet vortex generator with circular punched holes, Int. J. Heat Mass Tran. 209 (2023) 124142.
[41] S. Singh, S. Suman, S. Mitra, M. Kumar, Thermo-hydraulic performance enhancement of a solar air heater using rotating cylindrical turbulators, Appl. Therm. Eng. 236 (2024) 121748.
[42] S. Singh, S. Suman, S. Mitra, M. Kumar, Optimization of a novel trapezoidal staggered ribs configuration for enhancement of a solar air heater performance using CFD, Environ. Sci. Pollut. Control Ser. 30 (41) (2023) 93582–93601.
[43] A. Painuly, N.K. Mishra, P. Zainith, Thermo-hydraulic performance evaluation and comparison of SiC-MWCNT and Al2O3-MWCNT Non-Newtonian hybrid nanofluids using a heat exchanger equipped with helically corrugated tubes: an experimental study, J. Therm. Anal. Calorim. 149 (9) (2024) 3965–3980.
[44] S.R. Madas, R. Narayanan, P. Gudimetla, Numerical investigation on the optimum performance output of photovoltaic thermal (PVT) systems using nano-copper oxide (CuO) coolant, Sol. Energy 255 (2023) 222–235.
[45] A. Khelifa, M.E.H. Attia, Z. Driss, A.M. Manokar, Performance enhancement of photovoltaic solar collector using fins and bi-fluid: thermal efficiency study, Sol. Energy 263 (2023) 111987.
[46] A.M. Bassam, K. Sopian, A. Ibrahim, A.B. Al-Aasam, M. Dayer, Experimental analysis of photovoltaic thermal collector (PVT) with nano PCM and micro-fins tube counterclockwise twisted tape nanofluid, Case Stud. Therm. Eng. 45 (2023) 102883.
[47] A.B. Al-Aasam, A. Ibrahim, K. Sopian, B. Abdulsahib, M. Dayer, Nanofluid-based photovoltaic thermal solar collector with nanoparticle-enhanced phase change material (Nano-PCM) and twisted absorber tubes, Case Stud. Therm. Eng. 49 (2023) 103299.
[48] V.T. Rao, Y.R. Sekhar, M. Arıcı, N.R. Pochont, D.R. Prasad, Experimental investigations on bi-symmetrical web flow water based photovoltaic-thermal (PVT) system: energy, exergy, and entropy (3-E) analysis, Sol. Energy 271 (2024) 112445.
[49] M.R. Sharaby, M.M. Younes, F.S. Abou-Taleb, F.B. Baz, The influence of using MWCNT/ZnO-Water hybrid nanofluid on the thermal and electrical performance of a Photovoltaic/Thermal system, Appl. Therm. Eng. 248 (2024) 123332.